A New Application of Texture Unit Coding to Mass Classification for Mammograms

Yuan Chen and Chein-I Chang

Remote Sensing Signal and Image Processing Laboratory
Department of Computer Science and Electrical Engineering
University of Maryland, Baltimore County, Baltimore, MD 21250

ABSTRACT

Texture is one of important features of masses in mammograms. A recent texture unit-based texture spectrum approach, referred to as Texture Unit Coding (TUC) has shown promise in texture classification. This paper presents a new application of the TUC to mass classification in mammograms. The TUC generates a texture spectrum for a texture image that can be used to describe the characteristics of masses. It also develops an information divergence (ID)-based discrimination criterion to measure the discrepancy between two texture spectra, a concept yet to explore in texture analysis. The TUC along with ID are further applied to mass classification in mammograms where the MiniMammographic Database provided by the Mammographic Image Analysis Society (MIAS) is used for experiments.

1. INTRODUCTION

Texture is one of fundamental features to describe image characteristics. One commonly used approach is the spatial gray level co-occurrence matrix (SGLCM) that provides gray-level transition information between two gray levels.[1] Using a rather different approach,[2-4] Wang and He considered a 3×3 window as a texture unit (TU) along with its 8-neighbor connectivity[3] to generate an 8-dimensional texture feature vector for each pixel that represents the gray level changes between the center pixel of the texture unit, X_0 and its eight surrounding pixels labeled by X_1, X_2, X_3, X_4, X_5, X_6, X_7, X_8 considered to be neighboring pixels of X_0 shown in Fig. 1. As a result, each pixel can produce an 8-dimensional texture feature vector that describes gray-level changes in a texture unit along with these 8 orientations. Such an 8-dimensional texture feature vector can be further converted to a texture unit number (TUN) in a ternary representation that specifies a particular texture pattern. Because each pixel in an image generates its own TUN via a TU, these TUNs can be used to form a texture spectrum (TS) in the same way that gray level values of image pixels form an image histogram. The only difference is that the *x*-axis of the texture spectrum is specified by TUNs instead of the gray levels in the image histogram. By virtue of the texture spectrum, Wang and He have investigated various applications.[2-4] In this paper, we investigate a new application of TUC to mass classification in mammograms. Breast cancer is a leading cause of fatality among women. Mammography is by far the only effective screening procedure to detect breast cancer in early stage. Two main causes in breast cancer are calcifications and masses. In general, detection and classification of masses is considered to be more challenging than that of microcalcifications due to the fact that the masses are usually mixed with the inhomogeneous tissues in the breast background and the gray levels of these inhomogeneous tissues can vary with the breast tissues. It has been found that textures usually provide more reliable features in capture mammographic characteristics in detection and classification of masses. Over the past years, the SGLCM has been a major technique to extract texture features for mass detection and classification. The TUC provides a new alternative and produces new feature descriptors for mass classification. The two versions of TUC-based classification approaches are proposed, referred to as TUC1 and TUC2. The former uses the TS in conjunction with texture shape descriptors, while the latter implements TU-based texture feature descriptors followed by texture shape descriptors. In order to demonstrate the performance of TUC1 and TUC2 in mass classification, the SGLCM is used for comparison where the MIAS database is sued for experimental validation. Experiments show that both TUC1 and TUC2 perform better than the SGLCM-based approach.

2. TEXTURE UNIT CODING

Assume that V_0, V_1, V_2, V_3, V_4, V_5, V_6, V_7, V_8 are the gray levels corresponding to X_0, X_1, X_2, X_3, X_4, X_5, X_6, X_7, X_8 in Fig. 1 respectively, a texture feature number (TFN), E_i associated with a neighboring pixel X_i is defined by

$$E_i = \begin{cases} 0; \text{if } V_i < V_0 - \Delta \\ 1; \text{if } |V_i - V_0| \le \Delta \text{ for } i = 1, 2, \Lambda\, \Lambda, 8 \\ 2; \text{if } V_i > V_0 + \Delta \end{cases} \quad (1)$$

where Δ is a gray level tolerance to be determined. Since there are three values that an E_i in Eq. (1) can take, there are $3^8 = 6561$ combinations to cover all the possible values of (E_1, E_2, E_3, E_4, E_5, E_6, E_7, E_8), each of which can be specified by a number $N(E_1, E_2, E_3, E_4, E_5, E_6, E_7, E_8)$, referred to as texture unit number (TUN) of X_0, using the following ternary representation.

$$N(E_1, E_2, \Lambda, E_8) = \sum_{i=1}^{8} E_i \times 3^{i-1}. \quad (2)$$

By virtue of a TU, each image pixel can generate an 8-dimensional texture feature vector (E_1, E_2, E_3, E_4, E_5, E_6, E_7, E_8) from which a TUN can be produced using Eq. (2). Treating such a TUN as a gray level we can generate a texture spectrum for an image in a similar manner that a gray-level image histogram is generated for an image. Since each of eight orientations in Fig. 1 can be used to start off as the first neighboring pixel X_1, eight different texture spectra can be generated for each image. Using Eq. (2) we can further convert the TU-based texture spectrum to a probability distribution, p_{TUN} by

$$p_{\text{TUN}}(i) = N_{\text{TUN}}(i)/N \quad \text{for } i = 0, 1, \Lambda\ , 6560 \tag{3}$$

where $N_{\text{TUN}}(i)$ is the number of pixels whose TUN is $N(E_1, E_2, \Lambda\ , E_8) = i$ defined by Eq. (2) and N is the total number of pixels in the image.

3. INFORMATION DIVERGENCE

Since the TFN histogram of an image can be represented as a probability distribution by Eq. (3), we can use a well-known information measure, called information divergence[5] as a measure to describe the discrepancy between two images via their TFN histograms as follows. Let $\boldsymbol{\alpha}_m = \left(\alpha_{m,1}, \alpha_{m,2}, \Lambda\ , \alpha_{m,n_T}\right)^T$ and $\boldsymbol{\beta}_m = \left(\beta_{m,1}, \beta_{m,2}, \Lambda\ , \beta_{m,n_T}\right)^T$ be probability distributions of the TFN histogram of two images A and B respectively. Then the self-informations provided by image A and B for TFN = j are defined by $I_j(\boldsymbol{\alpha}_m) = -\log\alpha_{m,j}$ and $I_j(\boldsymbol{\beta}_m) = -\log\beta_{m,j}$ respectively. The self-information of $\boldsymbol{\beta}_m$ relative to the self-information of $\boldsymbol{\alpha}_m$ can be defined by

$$D(\boldsymbol{\alpha}_m \,\|\, \boldsymbol{\beta}_m) = \Sigma_j \alpha_{m,j} \log \alpha_{m,j}/\beta_{m,j} \tag{4}$$

which is called the relative entropy of $\boldsymbol{\beta}_m$ with respect to $\boldsymbol{\alpha}_m$, also known as Kullback-Leibler information measure.[5] Similarly, we can also define the average discrepancy in the self-information of $\boldsymbol{\alpha}_m$ relative to the self-information of $\boldsymbol{\beta}_m$ by

$$D(\boldsymbol{\beta}_m \,\|\, \boldsymbol{\alpha}_m) = \Sigma_j \beta_{m,j} \log \beta_{m,j}/\alpha_{m,j} \tag{5}$$

Summing Eqs. (4) and (5) yields Information Divergence (ID) defined by

$$\text{ID}(\boldsymbol{\alpha}_m, \boldsymbol{\beta}_m) = D(\boldsymbol{\alpha}_m \,\|\, \boldsymbol{\beta}_m) + D(\boldsymbol{\beta}_m \,\|\, \boldsymbol{\alpha}_m) \tag{6}$$

which can be used to measure the texture similarity between two texture images A and B. The ID offers a new look of texture similarity by taking advantage of relative entropy to account for the texture information provided by TFN histograms.

4. TEXTURE DESCRIPTORS

Two types of texture descriptors are considered in this section which will be used for mass classification, texture feature descriptors and texture shape descriptors.

4.1. Texture Feature Descriptors for TUC

The following texture feature descriptors proposed by Wang and He will be used to describe texture features extracted from the TUC in our experiments.[1]

1. Black-white symmetry (BWS):
$BWS = \left[1 - \Sigma_{i=0}^{3279}[S(i) - S(3281+i)]/\Sigma_{i=0}^{6560} S(i)\right] \times 100$
2. Geometric symmetry (GS):
$GS = \left[1 - 1/4\Sigma_{j=1}^{8}\left(\Sigma_{i=0}^{6560} S_j(i) - S_{j-1}(i)\right)/(2 \times \Sigma_{i=0}^{6560} S_j(i)\right)\right] \times 100$
3. Degree of direction (DD):
$DD = \left[1 - \left(1/6\right)\Sigma_{m=1}^{3}\Sigma_{n-m=1}^{4}\left(\Sigma_{i=0}^{6560}[S_m(i) - S_n(i)]/2\Sigma_{i=0}^{6560} S_m(i)\right)\right] \times 100$
4. Micro-Horizontal structure (MHS):
$MHS = \Sigma_{i=0}^{6560}\left[S(i) \times HM(i)\right]$
5. Central Symmetry (CS): $CS = \Sigma_{i=0}^{6560} S(i) \times \left[K(i)\right]^2$
6. $Entropy = -\Sigma_{i=0}^{6560} p_{\text{TUN}}(i) \log p_{\text{TUN}}(i)$

4.2. Texture Feature Descriptors for SGLCM

The SGLCM is generally specified by a displacement d and angular rotation θ. For any two gray level values, i and j, we define $N_{d,\theta}(i,j)$ as the total number of gray level transitions between any pair of two pixels whose gray level values i and j and which are d-pixel apart and specified by a angular rotation θ. We can obtain a probability distribution that describes the likelihood of gray level value i changed to gray level value j by normalizing $N_{d,\theta}(i,j)$ as follows.

$$p_{d,\theta}(i,j) = N_{d,\theta}(i,j)/\left(\Sigma_{i=0,j=0}^{L-1,L-1} N_{d,\theta}(i,j)\right) \tag{7}$$

Using Eq. (7), we can derive the following texture feature descriptors that have been widely used for mass classification.[1,6-7]

1. $ASM = \Sigma_{i=0}^{L-1}\Sigma_{j=0}^{L-1}\left[p_{d,\theta}(i,j)\right]^2$
2. $Inertia = \Sigma_{i=0}^{L-1}\Sigma_{j=0}^{L-1}(i-j)^2 p_{d,\theta}(i,j)$
3. $Correlation = \left\{\Sigma_{i=0}^{L-1}\Sigma_{j=0}^{L-1}\left[ijp_{d,\theta}(i,j)\right] - \mu_x\mu_y\right\}/\sigma_x\sigma_y$
4. $Entropy = -\Sigma_{i=0}^{L-1}\Sigma_{j=0}^{L-1} p_{d,\theta}(i,j) \log p_{d,\theta}(i,j)$
5. $SumEntropy = -\Sigma_k p_{sum}(k) \log p_{sum}(k)$ with
$p_{sum}(k) = \Sigma_{i=0}^{L-1}\Sigma_{j=0}^{L-1} p_{d,\theta}(i,j)$ for $k = i + j$
6. $DifferenceEntropy = -\Sigma_k p_{dif}(k) \log p_{dif}(k)$ with
$p_{dif}(k) = \Sigma_{i=0}^{L-1}\Sigma_{j=0}^{L-1} p_{d,\theta}(i,j)$ for $k = |\, i - j\,|$

4.3. Texture Shape Descriptors for TUC and SGLCM

Texture shapes provide very crucial information in specifying spiculated lesions. The following shape descriptors have been also used in mass classification.[8] Let R be the region of a mass.

1. $Circularity = area(R \cap C_{Eq})/area(R)$ with

$$R_{Eq} = \sqrt{area(C_{Eq})/\pi} = \sqrt{area(R)/\pi} = \sqrt{S/\pi}$$

where the circle C_{Eq} is one which has an area equal to the area of a mass, denoted by $S = area(R)$.

2. $RegionContrast = \left\{mean(R) - mean(\Omega)\right\} / mean(R)$ with a ring-like area Ω that indicates the circle band around the region of a mass calculated by $\Omega = \left\{(x, y) \mid d \le \sqrt{x^2 + y^2} \le d + \Delta d\right\}$
3. Radial Angle[8]
   Spiculated masses are usually an important indicator of being malignant masses. In order to capture this feature, the radial angle is used as a descriptor to differentiate the spiculation of a mass from the smoothness and roundness. The radial angle is the angle θ between the direction of the edge gradient and the radial direction of the edge as shown in Fig. 2, where the radial angle of P1 at the boundary of a mass is θ. As we can see, when the shape of a mass tends to be round, its radial angle will be close to 180^o, that is, the direction of the edge gradient tend to be the opposite to the radial direction of the edge. Conversely, a mass with spiculated edges will have smaller radial angles.
4. FWHM (Full Width at Half Maximum)[8]
   The FWHM is computed as the total number of angle values that is higher than half of the highest histogram value. When a histogram of radial angle is concentrated, the total number of radial angle values having their histogram larger than half of the highest histogram is smaller. Conversely, when the histogram distribution is spread, this total number of angle values is larger. Since the more irregular a mass is, the wider its histogram distribution of the radial angles, consequently, we will have the larger FWHM value.

5 EXPERIEMNTS

In this section, MIAS MiniMammographic Database provided by the Mammographic Image Analysis Society (MIAS) is used for experiments where the knowledge about the regions of interest is available. In this case, no mass detection is necessary so that we can focus on ability of each method to be evaluated in classification of masses. The mass classification is carried out by two stages, malignant/non-malignant classification followed by benign/normal classification. Three methods are evaluated for comparative analysis, which are TUC1: TUC with TS using ID in Section 3 and texture shape descriptors in Section 4.3, TUC2: TUC with texture feature descriptors in Section 4.1 and texture shape descriptors in Section 4.3 and SGLCM: SGLCM with texture feature descriptors in Section 4.2 and texture shape descriptors in Section 4.3. The difference between TUC1 and TUC2 is that TUC1 discriminates malignant masses from non-malignant tissues by measuring their texture spectra with ID, while TUC2 uses texture feature descriptors developed by Wang and He to do the same task. For fair comparison, the classifier used in these three methods is all the same which is a probabilistic neural network.[9] Additionally, the same shape descriptors in Section 4.3 are also applied to these three methods even though the shape features extracted from the TUC and SGLCM are different. 59 fatty mammograms in the MIAS database were selected for experiments, among which 13 are malignant, 18 are benign and 28 are normal. Fig. 3 shows examples of each of these three cases where images labeled by (a-c) are normal, benign and malignant lesions. Tables 1-3 tabulates the results for TUC1, TUC2 and SGLCM methods respectively where the tables labeled by (a) are the results yielded the 1st classification stage which were further processed in the 2nd classification stage to produce results in tables labeled by (b). Table 4 summarizes the average classification rates for each of three methods. According to Table 4, TUC1 was among the best which produced the highest classification rate, 71.18%. Compared to the worst rate, 40.68% that was yielded by the SGLCM method, the TUC1 performed significantly better than the SGLCM and slightly better than TUC2 which also had much better classification rate, 61.02% than did the SGLCM.

6 CONCLUSIONS

This paper investigates a utility of TUC in mass classification. The performance evaluation is conducted by using the same texture feature and shape descriptors along with the same classification network to ensure that the analysis is solely based on the effectiveness of texture features extracted from TUC and SGLCM. The experimental results demonstrate that the TUC-based approaches can be effective and perform better than the commonly used SGLCM-based methods. Since the performance of mass classification is determined by various factors such as texture descriptors and classifiers to be used, this paper only offers a new promising approach which has found success in remote sensing image processing and texture classification, but yet in mass classification. Many improvements can be made from the proposed TUC-based approaches such as selection of optimal sets of texture feature and shape descriptors and optimal classification networks.

References

1. R.M. Harlaick, K. Shanmugam, I. Dinstein, "Textural features for image classification," *IEEE Trans. System, Man and Cybernetics*. **3**(6), 610-621 (1973).
2. L. Wang and D.C. He, "A new statistical approach to texture analysis," *Photogrammetrics Engineering and Remote Sensing*. **56**, 61-65 (1990).
3. D.-C. He and L. Wang, "Texture unit, texture spectrum and texture analysis," *IEEE Trans. on Geoscience and Remote Sensing*. **28**(4), 509-512 (1990).
4. L. Wang and D.-C. He, "Texture classification using texture spectrum," *Pattern Recognition*. **23**(8), 905-910 (1990).

5. T. Cover and J. Thomas, *Elements of Information Theory*, John Wiley & Sons (1991).
6. I.E. Magnin, F. Cluzeau, C.L. Odet and A. Bremond, "Mammographic texture analysis: an evaluation of risk for developing breast cancer," *Optical Eng*., **25**(6), 780-784 (1986).
7. S.N.C. Cheng, H.P. Chan, M.A. Helvie and M.M. Goodsitt, "Classification of mass and nonmass regions on mammograms using artificial neural networks," *J. Imaging and Tech.*, **38**(6), 598-603 (1994).
8. Z. Huo, M.L. Giger, C.J. Vyborny, U. Bick, P. Liu, D.E. Wolverton and R.A. Schmidt, "Analysis of spiculation in the computerized classification of mammographic masses," *Med. Phys*., **22**, 1569-1579,. (1995).
9. D.F. Specht, "Probabilistic neural networks and the polynomial adaline as complementary techniques for classification," *IEEE Trans. Neural Networks*, **1**(1), 111-121 (1990).

X_4	X_3	X_2
X_5	X_0	X_1
X_6	X_7	X_8

Fig 1. Texture unit

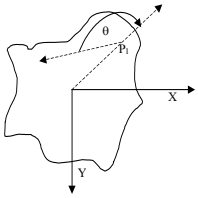

Fig 2. Radial angle

Fig 3. (a) normal (b) benign (c) malignant

Table 1(a). 1st stage classification by TUC1

	normal+benign (46 true cases)	malignant (13true cases)
normal+benign (47 test cases)	38	9
malignant (12 test cases)	8	4

Table 1(b). 2nd stage classification by TUC1 (38 cases)

	normal (23 cases from 1st stage)	benign (15 cases from 1st stage)
normal (23 test cases)	23	0
benign (15 test cases)	0	15

Table 2(a). 1st stage classification by TUC2

	normal+benign (46 true cases)	malignant (13true cases)
normal+benign (47 test cases)	37	10
malignant (12 test cases)	9	3

Table 2(b). 2nd stage classification by TUC2 (47 n+b cases and 10 malignant cases)

	normal (23 cases from 1st stage)	benign (14 cases from 1st stage)	malignant (10 cases from 1st stage)
normal (22 test cases)	20	1	1
benign (25 test cases)	3	13	9
malignant (0 test cases)	0	0	0

Table 3(a). 1st stage classification by SGLCM

	normal+benign (46 true cases)	malignant (13true cases)
normal+benign (37 test cases)	27	10
malignant (22 test cases)	19	3

Table 3(b). 2nd stage classification by SGLCM (27 n+b cases and 10 malignant cases)

	normal (17 cases from 1st stage)	benign (10 cases from 1st stage)	malignant (10 cases from 1st stage)
normal (22 test cases)	13	3	2
benign (25 test cases)	4	7	8
malignant (0 test cases)	0	0	0

Table 4. Average classification rates of TUC1, TUC2 and SGLCM methods

	normal	benign	malign ant	average classification rate
TUC1	0.8214	0.8333	0.3077	0.7118
TUC2	0.7143	0.7222	0.2308	0.6102
SGLCM	0.4643	0.4444	0.2308	0.4068